DOI: 10.31276/VJSTE.64(2).10-15

Effect of *in-situ* Fe doping on the visible light photoelectrochemical activity of TiO_2 nanorods

Nam Trung Tran*, Thi Minh Huong Pham, Tan Lam Nguyen

Faculty of Natural Sciences, Quy Nhon University

Received 5 February 2021; accepted 4 May 2021

Abstract:

Considering its superior photocatalytic activity and excellent chemical stability, titanium dioxide (TiO_2) is an excellent candidate for photoelectrochemical (PEC) hydrogen production. Besides, many challenges exist ahead of improving the photoresponse of TiO_2 to visible light while maintaining high photocatalytic activity. Herein, the authors report recent efforts to improve the visible light PEC activity of TiO_2 nanorods by *in-situ* doping with various iron (Fe) concentrations using a hydrothermal method. The influences of Fe doping concentrations on the morphological and structural properties of TiO_2 nanorods were investigated by using scanning electron microscopy (SEM), X-ray diffraction (XRD), and Raman spectroscopy. Furthermore, this work demonstrates that Fe doping could improve the PEC activity of TiO_2 nanorods under visible light irradiation. The authors achieve a remarkable enhancement in the photocurrent density, as high as 2.9 mA/cm^2 at an applied voltage of 0.5 V, for the sample synthesised with an Fe doping concentration of 10 mM. These results reveal that Fe-doped TiO_2 nanorods can serve as ideal materials for PEC applications.

Keywords: **Fe-doped TiO_2, hydrothermal, in-situ doping, photoelectrochemical, TiO_2 nanorods.**

Classification number: **2.1**

Introduction

PEC water splitting is one of the most promising and environmentally friendly approaches to providing clean and renewable energy. The process of water splitting comprises two half-cell reactions of water oxidation and proton reduction to hydrogen, which require a minimum energy of 1.23 eV to drive the reactions [1]. In a PEC system, the photoelectrode is a key component that plays an important role in capturing and converting solar energy directly to chemical energy in the form of hydrogen and oxygen. Various semiconducting materials such as TiO_2, ZnO, $BiVO_4$, Fe_2O_3… have been extensively explored as photoelectrodes for efficient PEC water splitting [2-4].

Over the few past decades, TiO_2 has become known as one of the most widely used materials for research applications related to environmental concerns and solar energy conversion. Recently, the use of a TiO_2-based photoelectrode for PEC water splitting has been considered as the superior candidate due to its strong photocatalytic activity, excellent chemical stability, and cost savings [5, 6]. However, low electron mobility, fast recombination of the photoexcited carriers, and wide band gap (~3.2 eV for anatase and ~3.0 eV for rutile phases) hampers the application of TiO_2 in photocatalytic materials [7]. Among the different strategies to overcome these drawbacks of TiO_2 photocatalysts, metal ion doping of TiO_2 is an effective strategy that improves its electronic properties, optical sensitivity, and photocatalytic activities. Existing research on metal ion doping of TiO_2 has recognised the critical role played by cation doping to extend the photoresponse of TiO_2 into the visible spectral range and to achieve more efficient photocatalytic properties. In particular, doping with metal ions tailors the energy bandgap and increases the electric conductivity of TiO_2 [8, 9]. Among metal ions such as Fe, Co, Mn, W, Ni, etc., the Fe(III) ion has attracted much attention as a dopant into the TiO_2 lattice due the similarity of their ionic radii [10]. In addition, doping with Fe can induce charge trapping levels in the energy band of TiO_2 and

*Corresponding author: Email: trannamtrung@qnu.edu.vn

promote the interfacial charge transfer process resulting in the prevention of charge carrier recombination [11]. Many approaches have been employed to dope TiO_2 nanostructures such as sol-gel methods, impregnation techniques, hydrothermal methods, or some combination of these [12, 13]. However, among these approaches, the use of hydrothermal methods have the advantage of achieving a good crystalline phase of the TiO_2 nanostructures, which is a benefit to thermal stability and photocatalytic activities.

In the present work, we report our recent efforts to understand the effects of Fe dopant concentration on TiO_2 nanorods. To achieve this, different doping concentrations of Fe were introduced into TiO_2 nanorods via an *in-situ* doping process using a hydrothermal method. The structural properties, morphologies, and optical properties of the obtained samples were characterised in detail. Moreover, the visible light PEC activities of the Fe-doped TiO_2 nanorods were investigated to evaluate the effect of Fe doping concentrations on the PEC performance of the TiO_2 nanorods.

Experimental design

Materials and synthesis

All chemicals were purchased from Sigma Aldrich and were used without further purification. Titanium butoxide ($C_{16}H_{36}O_4Ti$, >97%) was used as the TiO_2 precursor. Fe(III) nitrate nonahydrate ($Fe(NO_3)_3.9H_2O$, >98%) was used as the Fe source for doping the TiO_2 nanorods. The aqueous solutions were prepared using hydrochloric acid (HCl, 37%) and deionised (DI) water. Another solvent of ethanol (C_2H_5OH) was used for substrate cleaning.

Undoped TiO_2 and Fe-doped TiO_2 nanorods were prepared on fluorine-doped tin oxide (FTO) glass substrates in a Teflon-lined stainless steel autoclave using a hydrothermal method. The FTO substrates were cleaned prior to use by ultrasonication using ethanol and DI water, and subsequently dried under nitrogen gas. For the synthesis of the TiO_2 nanorods, an aqueous solution containing 0.2 ml of $C_{16}H_{36}O_4Ti$, 9 ml of HCl, and 9 ml of DI water was vigorously stirred until the solution became transparent. The mixture was then transferred to a 25-ml Teflon-lined stainless steel autoclave containing cleaned FTO substrates, followed by hydrothermal treatment at 180°C for 8 h. After the reaction was cooled down to room temperature, these samples were rinsed extensively with DI water and were dried under nitrogen gas. Finally, the samples were annealed in air at 500°C for 1 h. *In-situ* Fe-doped TiO_2 nanorods were prepared in a similar process except that certain amounts of $Fe(NO_3)_3.9H_2O$ were added into the mixed solution. The Fe dopant was used with 5, 10, and 20 mM molar concentrations, and the Fe-doped TiO_2 nanorods samples were denoted as T-Fe5, T-Fe10, and T-Fe20, respectively.

Characterisation and PEC measurement

The morphologies and structures of the synthesised samples were investigated by using SEM (Hitachi 4800) and XRD (Siemens D5000), respectively. The structural properties of the samples were investigated via micro-Raman spectroscopy using an excitation of 532 nm and a charge-coupled device detector.

A three-electrode system was assembled for the PEC measurement, which was performed in 1 M KOH electrolyte solution under simulated solar light with a 150 W xenon lamp (Newport 94021A). The reference and counter electrodes were made of Ag/AgCl and a Pt coil, respectively. Linear sweep voltammetry (LSV) and photocurrent-time scans were measured by an electrochemical analyser (DY2300 Series Potentiostat/Bipotentiostat, Digi-Ivy).

Results and discussion

XRD analysis

The structure of the synthesised materials was determined by XRD. Figure 1 shows the XRD patterns of the TiO_2 and Fe-doped TiO_2 samples with different Fe doping concentrations. The TiO_2 sample possesses diffraction patterns with strong characteristic peaks at 2θ angles of 26.8, 36.4, 41.6, 54.7, 63.1, and 70.2°, which can be assigned to (110), (101), (111), (211), (002), and (112) planes of the tetragonal rutile structure of TiO_2 (JCPDS No. 88-1175). The diffraction peaks of the FTO substrate were also observed and were marked by asterisk signs. The diffraction peaks of the Fe-doped TiO_2 samples with different Fe doping concentrations were all in good accord with the rutile phase of TiO_2. Additionally, any other crystalline phase containing metallic Fe or Fe oxides could not be observed. Compared to the pristine TiO_2 sample, the peaks of the Fe-doped TiO_2 sample were slightly broader and weaker. It is worth noting that

careful analysis of the main peak (110) of the rutile phase revealed a slight shift to lower angles for the Fe-doped TiO_2 sample, as can be seen from the inset of Fig. 1. It is also observed that the higher Fe doping concentration caused a larger shift toward lower angles. These shifts can be explained by the possible substitution of Ti^{4+} by Fe^{3+} in the crystal lattice of TiO_2. Due to the fact that the radius cation of Fe^{3+} (0.64 Å) is a little larger than that of Ti^{4+} (0.61 Å) [14], this replacement of Ti^{4+} by Fe^{3+} causes an increase in *d*-spacing that consequently causes a shift of the peak position to the lower angle side. Due to the change in the *d*-spacing, the crystal lattice of net TiO_2 was deformed, which resulted in a slightly weakened and broadened XRD peaks of the Fe-doped sample [15].

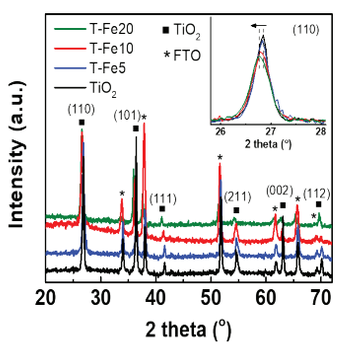

Fig. 1. XRD patterns of TiO_2 and Fe-doped TiO_2 nanorods on FTO substrates. The inset shows the peak (110) in the short range of diffraction angle.

Morphology

The morphologies and microstructures of the pristine and *in-situ* Fe-doped TiO_2 nanorod samples were investigated using SEM. Figure 2 shows SEM images of the undoped TiO_2 nanorods and Fe-doped TiO_2 nanorods with different Fe doping concentrations. It can be seen from Fig. 2A that the nanorods uniformly formed at a relatively high density with large spaces between each nanorod. These nanorods appear in tetragonal shapes with a square base and the diameter of each nanorod was ~250 nm. A cross-sessional SEM image of the TiO_2 sample reveals that vertically aligned nanorods were uniformly grown on the FTO substrate, and the film had a thickness of ~3.5 µm (Fig. 2E). When Fe dopant was introduced into the TiO_2 nanorod via *in-situ* doping of concentrations of 5 and 10 mM, the morphology of the doped samples remained the same as shown in Fig. 2A, i.e., the nanorods maintained their tetragonal shape (Figs. 2B and 2C). However, when increasing the doping concentration to 20 mM, larger nanorods formed at a higher density and thus the space between nanorods were narrower in this sample (Fig. 2D).

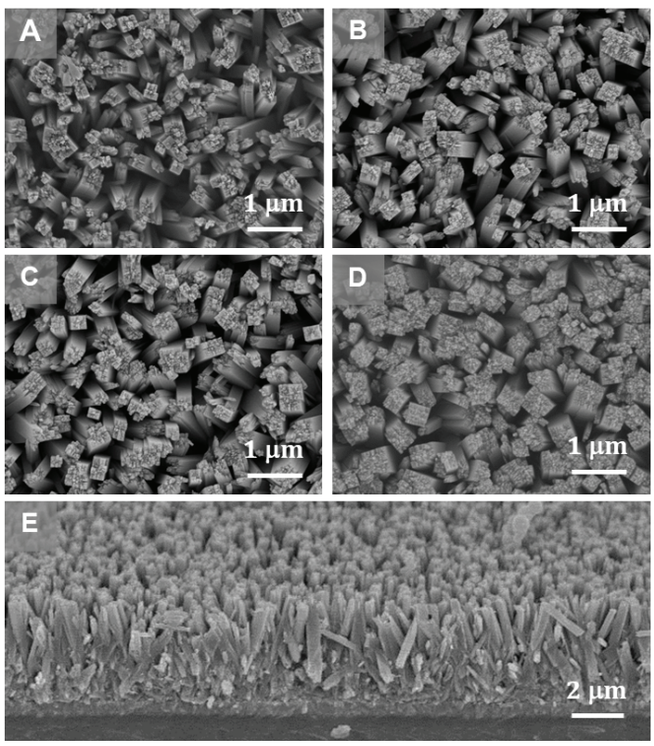

Fig. 2. SEM images of (A) undoped TiO_2 and Fe-doped TiO_2 with different doping concentrations of (B) 5, (C) 10, and (D) 20 mM; (E) cross-sessional SEM image of undoped TiO_2 nanorods.

Raman studies

To further investigate the structural properties and the effect of Fe doping on the TiO_2 nanorods, Raman spectroscopy was employed. It is well known that changes in Raman signals reflect a change of phase, bond, and/or structural defects in nanostructured materials [16, 17]. Figure 3 shows the Raman spectra of undoped and Fe-doped TiO_2 nanorods with different Fe doping concentrations. For the pristine TiO_2 nanorod sample, three typical Raman active modes were detected near 145, 447, and 612 cm^{-1}, which were assigned to the B_{1g}, E_g, and A_{1g} vibrational modes of the rutile phase of TiO_2. Another Raman peak positioned around 240 cm^{-1} was attributed to the second-order effect (SOE) [18]. All doped samples also exhibited the four vibrational modes, and no Raman peaks related to Fe or Fe compounds were detected. In addition, the E_g mode of the doped samples slightly decreased in Raman intensity and were

accompanied by a slight shift to lower wavenumbers (red shift) as shown in the inset of Fig. 3. The red shift of the E_g mode was attributed to internal strains caused by doping the TiO_2 structure [19]. This result indicated the substitution of Ti^{4+} by Fe^{3+} within the crystal lattice of rutile TiO_2 and reconfirms the results obtained from XRD.

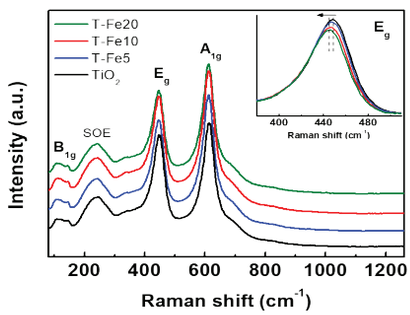

Fig. 3. Raman spectra of undoped TiO_2 and Fe-doped TiO_2 nanorods. The inset shows the Raman shift of the E_g mode in short range.

PEC performance

In order to investigate the effect of Fe doping concentration on the visible light PEC activity of the TiO_2 nanorods, photoelectrodes in the PEC cell were prepared from the synthesised samples. The working areas of all photoelectrodes were fixed at dimensions of 0.5×0.5 cm^2 by using non-conductive epoxy to cover the undesired area of the samples. LSV of the photoelectrodes was recorded under illumination of a solar light simulator to evaluate the PEC performance of the samples. Fig. 4A shows the current density-potential (J-V) curves of the undoped TiO_2 photoelectrode and Fe-doped TiO_2 photoelectrodes with different Fe doping concentrations of 5, 10, and 20 mM, hereafter referred to as the T-Fe5, T-Fe10, and T-Fe20 photoelectrodes, respectively. The PEC activity was greatly enhanced due to Fe doping into the TiO_2 nanorods. With an Fe doping concentration of 5 mM, the T-Fe5 photoelectrode showed a photocurrent density of 2.2 mA/cm^2 at an applied potential of 0.5 V, which was higher than that of the undoped TiO_2 photoelectrode (1.5 mA/cm^2 at 0.5 V) as shown in Fig. 4B. After increasing the Fe doping concentration to 10 mM, the photocurrent density of the T-Fe10 photoelectrode increased remarkably to 2.9 mA/cm^2 at 0.5 V. The photocurrent density of the T-Fe10 photoelectrode was comparable with those of previously reported metal-doped TiO_2 photoelectrodes such as Sn-doped TiO_2 nanowires (1.85 mA/cm^2 at 0 V) [20], Fe-doped bundled TiO_2 nanowires (0.88 mA/cm^2 at 0.8 V) [11], and Ta-doped TiO_2 nanorod arrays (0.67 mA/cm^2 at 1.23 V) [21]. However, the photocurrent density of the T-Fe20 photoelectrode reduced to 1.6 mA/cm^2 at 0.5 V upon Fe doping at a concentration of 20 mM. Therefore, it is evident that Fe doping concentration has a strong impact on the PEC performance of TiO_2 photoelectrodes.

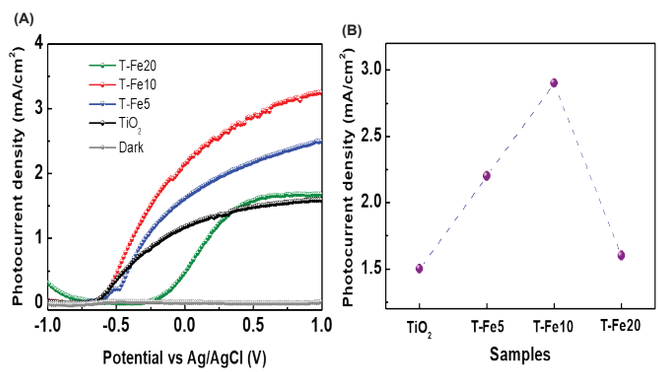

Fig. 4. (A) Photocurrent density-potential curves of undoped and Fe-doped TiO_2 nanorods with different doping concentrations; (B) Photocurrent density values of the photoelectrodes at an applied potential of 0.5 V (vs Ag/AgCl).

It is known that the PEC performance is dependent on the incident light absorption, the charge transfer and separation in the photoelectrodes, and the injection of charge from the material's surface to the electrolyte [22]. An enhancement in the PEC performance of the Fe doping photoelectrodes could be explained by considering the efficient separation and transfer of photoexcited charge. As discussed above, upon Fe doping into the TiO_2 nanorods, Ti^{4+} was substituted by Fe^{3+}. Because the energy band levels for Fe^{3+} are above the valence band level of TiO_2 (Fig. 5), Fe^{3+} can act as photogenerated hole trappers and transform into Fe^{4+} ions. Since Fe^{4+} ions are relatively unstable compared to Fe^{3+} ions, the trapped holes can be easily released from the Fe^{4+} ions and can migrate to the surface to participate in the redox reactions, which therefore enhance the PEC activity [23]. Nevertheless, Fe^{3+} may act as recombination centres for electrons and holes. Therefore, upon high doping concentration, more recombination centres are generated that compete with the redox reactions and result in a reduction of the PEC activity of the photoelectrode.

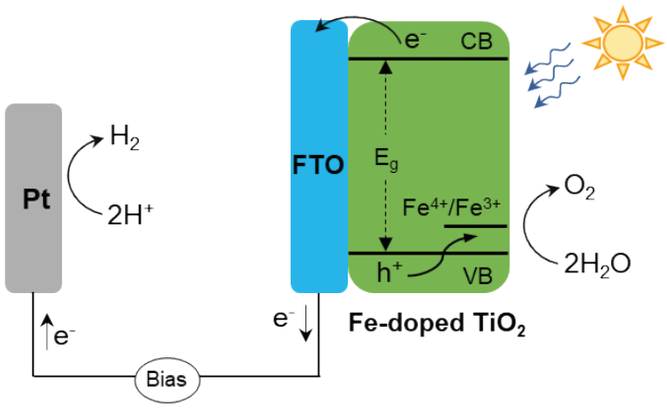

Fig. 5. Schematic of the energy level diagram for the charge transfer processes in the Fe-doped TiO_2 nanorods.

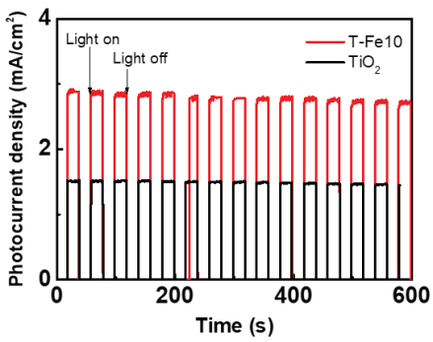

Fig. 6. Photocurrent-time scans of the undoped TiO_2 sample and Fe-doped TiO_2 sample with 10 mM Fe doping concentration (T-F10) at an applied potential of 0.5 V (vs Ag/AgCl). The duration for light on/light off is 20 s/20 s.

To evaluate the long-term stability of the PEC reaction of the Fe-doped TiO_2 nanorods, photocurrent-time (I-t) scans were recorded as shown in Fig. 6. It can be seen from the figure, these samples exhibited outstanding long-term stability. In addition, the instantaneous increase or decrease in the photocurrent at the transition from light-on to light-off indicated that the electron-hole pairs immediately generated and then separated in the TiO_2 nanorods, respectively. Thus, these results suggest effective charge separation and transfer in the TiO_2 nanorods, and a relatively long electron lifetime in the Fe-doped TiO_2 nanorods.

Conclusions

The *in-situ* Fe-doped TiO_2 nanorods with different Fe doping concentrations were synthesised on FTO substrates via the hydrothermal method. XRD and Raman results confirmed the success of Fe doping in which Ti^{4+} was substituted by Fe^{3+} in the crystal lattice of TiO_2. The synthesised samples showed great performance of visible light PEC activity. The Fe-doped TiO_2 nanorods with 10 mM Fe doping concentration exhibited a remarkable improvement in the photocurrent density (2.9 mA/cm^2) compared to that of the undoped TiO_2 sample (1.5 mA/cm^2). This enhanced PEC performance of the Fe-doped TiO_2 nanorod sample was ascribed to effective carrier separation and transfer due to the energy mechanism of Fe^{3+} and TiO_2. These results revealed that Fe-doped TiO_2 nanorods can serve as potential photoelectrode materials for PEC applications.

ACKNOWLEDGEMENTS

This research is funded by Vietnam National Foundation for Science and Technology Development (NAFOSTED) under grant number 103.02-2018.329.

COMPETING INTERESTS

The authors declare that there is no conflict of interest regarding the publication of this article.

REFERENCES

[1] M.G. Walter, et al. (2010), "Solar water splitting cells", *Chemical Reviews*, **110(11)**, pp.6446-6473.

[2] K.H. Ye, et al. (2019), "Enhancing photoelectrochemical water splitting by combining work function tuning and heterojunction engineering", *Nature Communications*, **10**, DOI: 10.1038/s41467-019-11586-y.

[3] L. Wang, et al. (2014), "Enhancing the water splitting efficiency of Sn-doped hematite nanoflakes by flame annealing", *Chemistry*, **20(1)**, pp.77-82.

[4] J.S. Yoon, et al. (2019), "Enhanced photoelectrochemical properties of Z-scheme ZnO/p-n Cu_2O PV-PEC cells", *Journal of Alloys and Compounds*, **771**, pp.869-876.

[5] J. Tian, et al. (2014), "Recent progress in design, synthesis, and applications of one-dimensional TiO_2 nanostructured surface heterostructures: a review", *Chem. Soc. Rev.*, **43(20)**, pp.6920-6937.

[6] M. Ge, et al. (2016), "A review of one-dimensional TiO_2 nanostructured materials for environmental and energy applications", *Journal of Materials Chemistry A*, **4(18)**, pp.6772-6801.

[7] S. Shen, et al. (2018), "Titanium dioxide nanostructures for photoelectrochemical applications", *Progress in Materials Science*, **98**, pp.299-385.

[8] H. Feng, et al. (2012), "Hydrothermal synthesis and photocatalytic performance of metal-ions doped TiO_2", *Applied Catalysis A: General*, **413-414**, pp.238-244.

[9] S.M. Adyani, M. Ghorbani (2018), "A comparative study of physicochemical and photocatalytic properties of visible light responsive Fe, Gd and P single and tri-doped TiO_2 nanomaterials", *Journal of Rare Earths*, **36(1)**, pp.72-85.

[10] J. Chen, et al. (2015), "Recent progress in enhancing photocatalytic efficiency of TiO_2-based materials", *Applied Catalysis A: General*, **495**, pp.131-140.

[11] W. Chakhari, et al. (2017), "Fe-doped TiO_2 nanorods with enhanced electrochemical properties as efficient photoanode materials", *Journal of Alloys and Compounds*, **708**, pp.862-870.

[12] N. Nithya, et al. (2018), "Neodymium doped TiO_2 nanoparticles by sol-gel method for antibacterial and photocatalytic activity", *Materials Science in Semiconductor Processing*, **83**, pp.70-82.

[13] J.A. Navío, et al. (1998), "Heterogeneous photocatalytic reactions of nitrite oxidation and Cr(VI) reduction on iron-doped titania prepared by the wet impregnation method", *Applied Catalysis B: Environmental*, **16(2)**, pp.187-196.

[14] R.D. Shannon (1976), "Revised effective ionic radii and systematic studies of interatomic distances in halides and chalcogenides", *Acta Crystallographica Section A*, **32(5)**, pp.751-767.

[15] J. Zhu, et al. (2006), "Fe^{3+}-TiO_2 photocatalysts prepared by combining sol–gel method with hydrothermal treatment and their characterization", *Journal of Photochemistry and Photobiology A: Chemistry*, **180(1)**, pp.196-204.

[16] Alamgir, et al. (2014), "Structural phase analysis, band gap tuning and fluorescence properties of Co doped TiO_2 nanoparticles", *Optical Materials*, **38**, pp.278-285.

[17] D. Komaraiah, et al. (2019), "Structural, optical and photoluminescence studies of sol-gel synthesized pure and iron doped TiO_2 photocatalysts", *Ceramics International*, **45(18)**, pp.25060-25068.

[18] V. Swamy, et al. (2006), "Size-dependent modifications of the Raman spectrum of rutile TiO_2", *Applied Physics Letters*, **89(16)**, DOI: 10.1063/1.2364123.

[19] Y. Zhang, et al. (2013), "Asymmetric lattice vibrational characteristics of rutile TiO_2 as revealed by laser power dependent Raman spectroscopy", *The Journal of Physical Chemistry C*, **117(45)**, pp.24015-24022.

[20] M. Xu, et al. (2012), "Controlled Sn-doping in TiO_2 nanowire photoanodes with enhanced photoelectrochemical conversion", *Nano Letters*, **12(3)**, pp.1503-1508.

[21] S. He, et al. (2018), "Hierarchical Ta-doped TiO_2 nanorod arrays with improved charge separation for photoelectrochemical water oxidation under FTO side illumination", *Nanomaterials (Basel, Switzerland)*, **8(12)**, DOI: 10.3390/nano8120983.

[22] G. Wang, et al. (2015), "Significantly enhanced visible light photoelectrochemical activity in TiO_2 nanowire arrays by nitrogen implantation", *Nano Letters*, **15(7)**, pp.4692-4698.

[23] J. Zhu, et al. (2004), "Characterization of Fe-TiO_2 photocatalysts synthesized by hydrothermal method and their photocatalytic reactivity for photodegradation of XRG dye diluted in water", *Journal of Molecular Catalysis A: Chemical*, **216(1)**, pp.35-43.